On Mutual Information of Measured 60 GHz Wideband Indoor MIMO Channels: Time Domain Singular Values

BLUMENSTEIN, J.; MARŠÁLEK, R.; GÖTTHANS, T.; NISSEL, R.; RUPP, M.

IIEEE International Symposium on Personal, Indoor and Mobile Radio Communications (IEEE PIMRC 2017)

eISBN: 978-1-5386-3529-2

DOI: https://doi.org/10.1109/PIMRC.2017.8292754

Accepted manuscript

On Mutual Information of Measured 60 GHz Wideband Indoor MIMO Channels: Time Domain Singular Values

Jiri Blumenstein†, Roman Marsalek†, Tomas Gotthans†, Ronald Nissel‡ and Markus Rupp‡
†The Faculty of Electrical Engineering and Communication, Brno Univ. of Technology, Czech Rep.
‡Christian Doppler Lab. for Dependable Wireless Connectivity for the Society in Motion, TU Wien, Austria
Email: {blumenstein, marsaler, gotthans}@vutbr.cz, {rnissel, mrupp}@nt.tuwien.ac.at

***Abstract*—This paper presents a report on mutual information based on measured indoor millimeter-wave (mmWave) channels with multiple antennas at input and output (MIMO). We show that for fixed indoor communication systems, an optimal antenna element spacing can be found such that the measured mutual information almost reaches the capacity of a perfectly orthogonal (theoretical) MIMO channel (with the same number of receiver (RX) and transmitter (TX) antennas). Secondly, we present, that even though the measured channel transfer functions (CTFs) exhibit large fluctuations (i.e., temporal dispersion), the mutual information is mainly determined by the mean singular value of the line-of-sight (LOS) components. Due to their strong variations over frequency mmWave channels are tedious when describing them with classical methods in the frequency domain. An approximation by numerous flat subbands leads to an error in mutual information (MI) by 2bit/s/Hz (for 80% probability). In comparison, our proposed method in the time domain, however, offers a notably smaller error (1bit/s/Hz for 80% probability).**

I. Introduction

With the lasting upswing of required data rates of almost all communication systems, the utilization of new and unused frequency bands is a must [1]. Recognized and promising is the millimeter-wave (mmWave) band which we consider to span from 55 to 65 GHz. As defined by many spectrum managing authorities, the mmWave band to some extent overlaps the un-licensed industrial scientific and medical (ISM) bands and therefore it is especially attractive for both industry and the research community. On the other hand, mmWave hardware based on gallium arsenide technology comes with a notably higher price than the widespread silicon based technology [2]. One of the proposed solution to lower the price of the mmWave multiple-input multiple-output (MIMO) transceivers is to utilize the spatial modulation (SM), while supporting MIMO, it requires only one radio-frequency (RF) chain [3]. Thus, mmWave SM could represent a cost effective solution for some areas of the wireless communication.

978-1-5386-3531-5/17/$31.00

The efficient implementation of mmWave SM MIMO system requires non-mobile line-of-sight (LOS) propagation conditions together with optimal antenna elements spacing. The antenna element spacing is proportional to propagation distance as well as wavelength according to [4]

$$\zeta \approx \sqrt{\frac{D\lambda}{N}}, \tag{1}$$

where ζ is the antenna element spacing, D is the RX-TX distance, N is the number of antenna elements and λ is the wavelength. Please note that relation (1) represents a simplified solution where perfectly parallel uniform linear arrays (ULAs) with the same number of elements N are used.

This paper deals with the channel characterization of mmWave MIMO channels while the details regarding system design using SM scheme can be found in [4], [5]. In the field of the mmWave channel sounding, an extensive research has been done in the last two decades, e.g. [6]–[8], but for SM, the utilized measurement setups are not optimal mainly in terms of the critical antenna element spacing.

Also, as recently published in [9], where research questions regarding the fundamental mmWave channel capacities have been opened. However, while no real-world measurement aiming at the specifics of the SM scheme has been performed, the contribution of this paper is following:

- We present a channel sounding campaign capturing in total 11 measurement scenarios while over 200 channel transfer functions (CTFs) were recorded for 4×4 and 6×6 MIMO configurations.
- We analyzed the measured mutual information (MI) dependency on 1) bandwidth, 2) antenna element separation and 3) multipath richness of the 60 GHz indoor channel with 10 GHz bandwidth.
- We demonstrate a relation between the overall MI of the channel and the mean singular value of the LOS components.

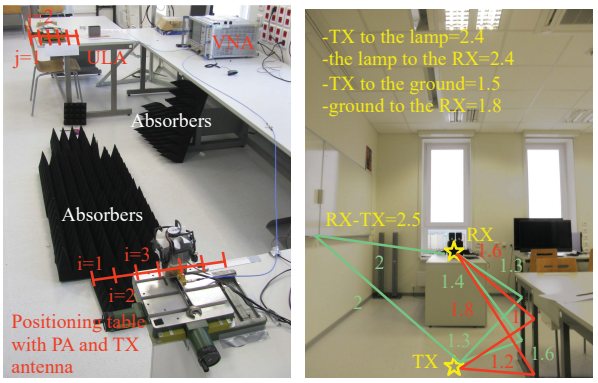

(a) Measurement site I (b) Measurement site II

Fig. 1: Photographs of two out of three measurement locations. Measurement site III is similar to the site II, but the xy tables (emulating the ULAs as in [8]) are placed on top of the desk with 12 cm antenna height from the surface. All dimensions are in meters.

II. Measurement

A. Measurement locations

The measurement campaign was carried out in the laboratory environment at Brno University of Technology. We have measured mmWave channels in three different sites, where site I and site II are depicted in Figure 1. The difference between the measurement sites is mainly in the multipath richness of the recorded CTFs. Site I features the lowest amount of multipath components (MPCs) due to the absorbing materials covering major reflective surfaces. Site II is without absorbing materials while the ULAs are positioned such that in their near proximity, metallic constructions of the tables are present. This causes a notable increase of the MPCs. Measurement site III was located in the same office as the site II, with the main difference that the ULAs were placed on the top of the tables visible on the right hand side of Figure 1b.

We utilized a 4×4 MIMO setup configured with an element separation $\boldsymbol{\zeta} \in [\zeta, \frac{\zeta}{\sqrt{2}}, \frac{\zeta}{2}]$. For detailed information about the MIMO configurations and element separations, please see Table I, where all separations are determined with a center frequency $f = 60$ GHz.

TABLE I: List of antenna element separations used for selected MIMO configuration and measurement sites. Calculated using Eq. 1

$\boldsymbol{\zeta}$	Site I, II for $D = 3$m		Site III for $D = 2.5$m
	4×4	6×6	4×4
ζ	61.24 mm	3,32 mm	35.3 mm
$\frac{\zeta}{\sqrt{2}}$	43.30 mm	-	25.0 mm
$\frac{\zeta}{2}$	30.61 mm	-	17.6 mm

B. 55–65 GHz Channel sounder

The channel sounder consists of a vector network analyzer (VNA) and the transmitter (TX) and receiver (RX) antenna. As the channel is time invariant, we are allowed to emulate the MIMO setup by changing the positions of the TX and RX antennas utilizing the precise xy-tables on both RX and TX sides. The channel sounder operates on the frequency domain principle described in [7], [8] (The time-domain mmWave sounder is demonstrated in [10]). In this frequency-domain method, a narrow-band continuous wave signal is transmitted via the channel and the signal is swept from 55 to 65 GHz with a step size of 10 MHz.

III. Data acquisition and processing

A. Channel transfer functions

Unlike with correlative channel sounding, the frequency domain channel data acquisition is straightforward according to

$$\tilde{h}_{ji}(f) = s^{21}_{ji}(f), \tag{2}$$

where f is an index to the discrete measurement frequencies, i, j are, respectively, the indices of the antenna elements of the virtual ULAs, and s^{21} is the S-parameter, representing the transmission from the TX antenna to the RX antenna. Utilizing the inverse Fourier transform (IFT), we transform the CTF matrix

$$\mathbf{H}(f) = \begin{pmatrix} \tilde{h}_{11}(f) & \tilde{h}_{12}(f) \\ \tilde{h}_{21}(f) & \tilde{h}_{22}(f) \end{pmatrix} \tag{3}$$

into the channel impulse response (CIR) as

$$h_{ji}(\tau) = \sum_{f=0}^{L-1} \tilde{h}_{ji}(f) \exp\left(j \frac{2\pi f \tau}{N}\right), \tag{4}$$

where $h_{ji}(\tau)$ is the ji-th element of the multipath channel matrix $\mathbf{H}(\tau)$ constructed in a same manner as shown in Equation (3) for $\mathbf{H}(f)$ and τ is an index to the corresponding time instances.

B. Frequency flat subbands of the CTFs

In order to determine the MI of the frequency selective channel, we partition the measured bandwidth $\mathcal{W}$ into n frequency flat subbands according to

$$B_{n\,\mathrm{flat}}(f_1, f_2, r) = \Big\{ \Delta f \,\Big|\, \Big(|\tilde{h}_{ji}(f_2)| > |\tilde{h}_{ji}(f_1)| - \frac{r}{2}, \; |\tilde{h}_{ji}(f_2)| < |\tilde{h}_{ji}(f_1)| + \frac{r}{2} \Big) \Big\} \tag{5}$$

such that $B_{n\,\mathrm{flat}}(f_1, f_2, r)$ forms a continuously sampled spectral space, $\Delta f = f_2 - f_1$ and $f_1 < f_2$ where both are limited to the measured frequencies. The tolerance threshold r defines the flatness of the subband. In the following, we utilize $r \in [1.4, 3, 5]$ dB. As a result, all

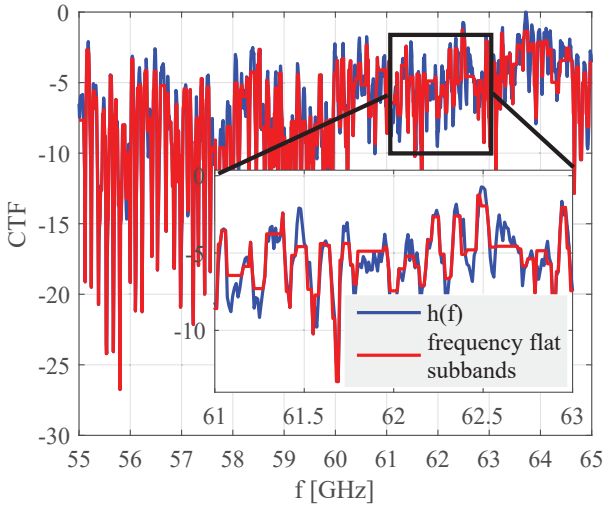

Fig. 2: Typical CTF. The red piecewise linear curve represents the frequency flat subbands.

frequency components within the flat fading subband experience the same magnitude of fading with the maximal difference of r. Then, the measured bandwidth $\mathcal{W}$ is composed of n the subbands by

$$\mathbf{B}_{\text{flat}}(f,r) = [B_{1\,\text{flat}}(f_1,f_2,r), B_{2\,\text{flat}}(f_2,f_3,r), ...]^T. \tag{6}$$

Now, the MIMO channel matrix $\mathbf{H}(f)$ is approximated with

$$\mathbf{H}''(f,r) = \mathbf{H}(\mathbf{B}_{\text{flat}}(f,r)). \tag{7}$$

A graphical representation of the resulting piecewise linear (frequency flat) subband curve is plotted in Figure 2.

C. Frequency domain mutual information determination

As outlined in [11], [12], utilizing the CTF matrix $\mathbf{H}(f)$, the MI of the frequency selective MIMO channel is given by

$$I_\gamma = \frac{1}{\mathcal{W}} \sum_f \log_2 \det(\mathbf{I} + \frac{\gamma}{N}\mathbf{H}(f)\mathbf{H}(f)^H), \tag{8}$$

where $\mathbf{I}$ is an identity matrix and γ is the signal-to-noise ratio (SNR).

In Figure 3, the effect of the antenna separation for $\boldsymbol{\zeta} \in [\zeta, \frac{\zeta}{\sqrt{2}}, \frac{\zeta}{2}]$ is plotted. For the sake of comparison, we also plot the MI function of a perfectly orthogonal LOS (simulated via identity matrix, representing an upper bound of a theoretical channel) and Rayleigh fading.

1) Impact on the antenna element separation: From Figure 3 we read that for γ=20 dB, I_γ=30.60 bit/s/Hz for the orthogonal LOS channel (identity channel), while for the measured channel with the optimal antenna separation I_γ=27.82 bit/s/Hz, so to the upper limit of a theoretical channel, there remains 2.78 bit/s/Hz (≈8.9% decrease). The smaller the element separation, the lower the MI I_γ=23.40 bit/s/Hz (≈23.5% decrease) and finally

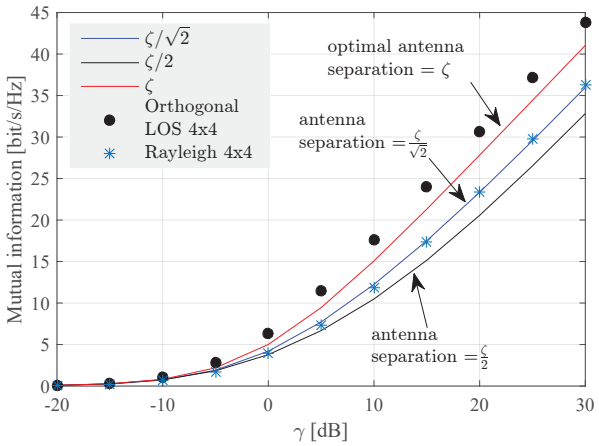

Fig. 3: Variations of the antenna element separation and the effect on the MI. Measurement site I, 4×4.

I_γ=20.57 bit/s/Hz (≈ 32.7% decrease) for the smallest element separation.

2) Impact on the bandwidth: We measure the channel with a bandwidth of 10 GHz while the orthogonality condition Eq. (1) holds only for the center frequency 60 GHz. Therefore, the orthogonality is impaired, the wider the measured bandwidth. This is visible in Figure 4. For γ=20 dB, and a bandwidth of 1 GHz, I_γ=27.82 bit/s/Hz, i.e., 2.83 bit/s/Hz higher then for the case with 10 GHz bandwidth. All the so far mentioned values are for Measurement site I, which has the lowest amount of MPCs.

3) Impact of the Measurement site: In Figure 4 we can also observe the MI function for Measurement site III. It is seen, thanks to the stronger reflections, thus impaired orthogonality, the MI is lower by 1 bit/s/Hz @ BW=1 GHz. For BW=10 GHz, the difference is 3 bit/s/Hz.

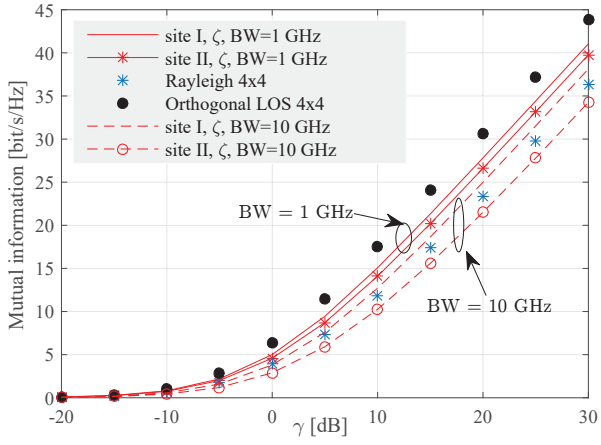

Fig. 4: Influence of the bandwidth BW $= [1, 10]$ GHz. The center frequency $f_c = 60$ GHz.

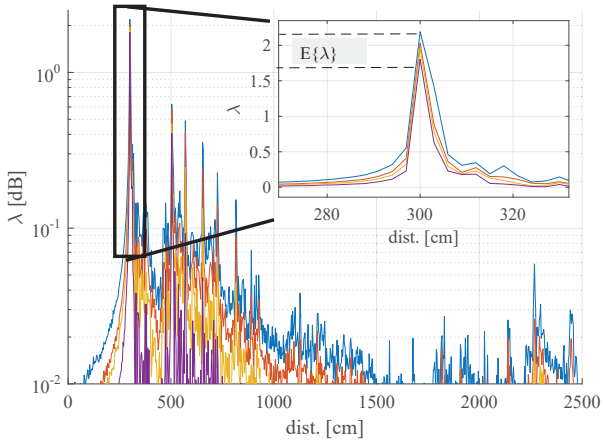

Fig. 5: The time evolution of the singular values of selected data set (4×4, site I, ζ). The x-axis is scaled to the distance and is easy remapped to the delay via $\tau = c/\text{dist.}$, $c = 3 \times 10^8$ m/s.

D. Time domain mutual information determination

Unlike the traditional application of the singular value decomposition (SVD), which is performed in the frequency domain, we define the channel singular values in the delay domain as:

$$\text{SVD}(\mathbf{H}(\tau)) \rightarrow \boldsymbol{\lambda}(\tau), \tag{9}$$

where

$$\boldsymbol{\lambda}(\tau) = [\lambda_{1,1}(\tau), \lambda_{2,2}(\tau), ..., \lambda_{N,N}(\tau)]. \tag{10}$$

Now, given the circumstances of the measurements, the LOS components are obtained as

$$\lambda_{\text{LOS}\,ji} = \max_{\tau} \lambda_{ji}(\tau). \tag{11}$$

The delay domain evolution of $\lambda_{ji}(\tau)$ is visible in Figure 5 highlighting the LOS components.

Now, utilizing all measured datasets, which amounts in total 11 measurements, we show that the MI is related to the mean singular values of the LOS component, i.e.

$$I''_\gamma \propto \mathbb{E}\{\lambda_{\text{LOS}\,ji}\} = \frac{1}{N} \sum_{ji} \lambda_{\text{LOS}\,ji}. \tag{12}$$

Intuitively, this can be explained by the fact that the main singular value contains most of the energy and thus reflects well the channel behavior in terms of MI.

In Figure 6a we plot the measured $I_\gamma = f(\mathbf{H}(f), \gamma)$ for $\gamma = 20\,\text{dB}$ and its exponential fit

$$I''^{\text{D}}_\gamma = a(\gamma) \exp\{b(\gamma)\, \mathbb{E}\{\lambda_{\text{LOS}}\}\} \tag{13}$$

obtained via a maximum likelihood estimation (MLE). The parameters $a(\gamma), b(\gamma)$ of fit (13) are plotted in Figure 6b. The superscript $^{\text{D}}$ designates the calculation from the delay domain.

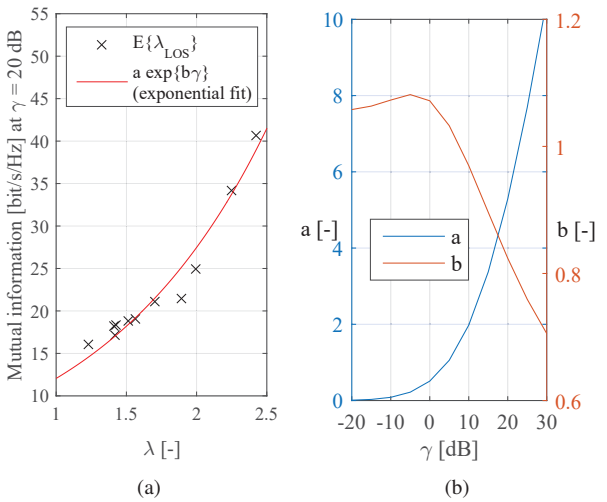

(a) (b)

Fig. 6: (a) Dependency of the I_γ, the measured mean singular value of the LOS component $\mathbb{E}\{\lambda_{\text{LOS}}\}$ and its exponential fit
(b) Two parameters of the exponential mapping function (13).

IV. Validation

To validate the proposed mapping (13), we define an error magnitude

$$\epsilon = |I_\gamma - I''_\gamma| \text{ and } \epsilon^{\text{D}} = |I_\gamma - I''^{\text{D}}_\gamma|, \tag{14}$$

where $I_\gamma = f(\mathbf{H}(f), \gamma)$ and $I''_\gamma = f(\mathbf{H}''(f, r), \gamma)$ are evaluated via (8) utilizing the frequency domain data. To evaluate the the mutual information from the temporal domain data, I''^{D}_γ is determined by (13).

The cumulative distribution functions (CDFs) of ϵ and ϵ^{D} are depicted in Figure 7. It is visible, that for the threshold $r = 3\,\text{dB}$ and $r = 5\,\text{dB}$, the precision of the MI evaluation is notably lower compared to the proposed mapping (13). To obtain approximately equal precision, we set $r = 1.4\,\text{dB}$. This, however, represents several hundreds of $\tilde{h}_{ji}(f)$ coefficients.

V. Conclusion

We conclude that:

1) The MI of the measured channels with optimal antenna element separation is close (with 8.9% difference) to the MI of the identity matrix (i.e. the capacity of an ideally decoupled MIMO channel). Thus, for intended application, proper ULA design is of paramount importance.

2) The higher the bandwidth, the lower the MI due to orthogonality disturbance caused by increasing suboptimality antenna element separation.

3) The MI can be estimated from the mean singular value of the LOS component with good precision. In fact, when the MI is calculated as the sum of its individual contributions from the number of frequency

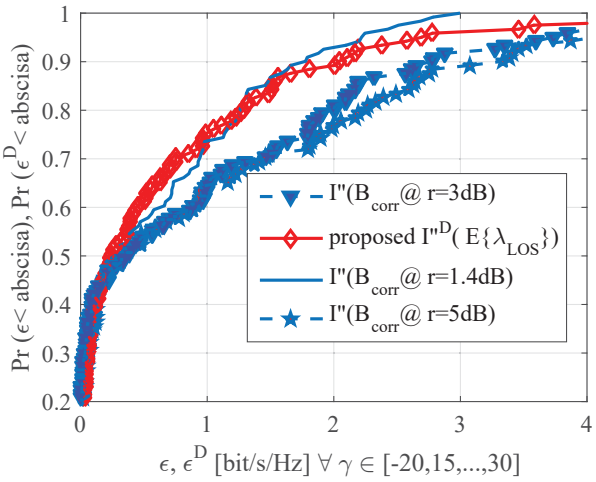

Fig. 7: CDF of the MI estimate error for the proposed technique and three traditional techniques based on the frequency flat subbands with the threshold $r \in \{1.4, 3, 5\}$ dB.

flat subbands, the channel gain variation inside of each subband has to be as low as 1.4 dB, in order to obtain approximately the same MI accuracy as through the proposed method.

ACKNOWLEDGMENT

Research described in this paper was financed by Czech Science Foundation project 17-18675S *Future transceiver techniques for the society in motion* and partially supported by the Czech Ministry of Education in frame of National Sustainability Program under grant LO1401. For research, infrastructure of the SIX Center was used.

REFERENCES

[1] T. S. Rappaport, S. Sun, R. Mayzus, H. Zhao, Y. Azar, K. Wang, G. N. Wong, J. K. Schulz, M. Samimi, and F. Gutierrez, "Millimeter wave mobile communications for 5G cellular: It will work!" *IEEE access*, vol. 1, pp. 335–349, 2013.

[2] B. Adelseck, J. Schroth, U. Meiners, and P. Quentin, "Effects of MMIC-design and GaAs technology on mm-Wave module production yield," in *2000 30th European Microwave Conference*, Oct 2000, pp. 1–4.

[3] M. Di Renzo, H. Haas, A. Ghrayeb, S. Sugiura, and L. Hanzo, "Spatial modulation for generalized MIMO: Challenges, opportunities, and implementation," *Proc. IEEE*, vol. 102, no. 1, pp. 56–103, Jan. 2014.

[4] P. Liu, M. Di Renzo, and A. Springer, "Line-of-sight spatial modulation for indoor mmWave communication at 60 GHz," *IEEE Trans. Wireless Commun.*, vol. 15, no. 11, pp. 7373–7389, Nov. 2016.

[5] ——, "Variable-N_u generalized spatial modulation for indoor LOS mmWave communication: Performance optimization and novel switching structure," *IEEE Trans. on Commun.*, vol. PP, no. 99, pp. 1–16, 2017.

[6] A. Maltsev, R. Maslennikov, A. Sevastyanov, A. Khoryaev, and A. Lomayev, "Experimental investigations of 60 GHz WLAN systems in office environment," *IEEE J. Sel. Areas Commun.*, vol. 27, no. 8, pp. 1488–1499, Oct. 2009.

[7] A. Chandra, A. Proke, T. Mikulek, J. Blumenstein, P. Kukolev, T. Zemen, and C. F. Mecklenbruker, "Frequency-domain in-vehicle UWB channel modeling," *IEEE Trans. Veh. Technol.*, vol. 65, no. 6, pp. 3929–3940, June 2016.

[8] J. Blumenstein, A. Prokes, A. Chandra, T. Mikulasek, R. Marsalek, T. Zemen, and C. Mecklenbruker, "In-vehicle channel measurement, characterization, and spatial consistency comparison of 3-11 GHz and 55-65 GHz frequency bands," *IEEE Trans. Veh. Technol.*, vol. 66, no. 5, pp. 3526–3537, May 2017.

[9] G. C. Ferrante, T. Q. Quek, and M. Win, "Revisiting the capacity of noncoherent fading channels in mmWave system," *IEEE Trans. Commun.*, 2017.

[10] J. Blumenstein, J. Vychodil, M. Pospisil, T. Mikulasek, and A. Prokes, "Effects of vehicle vibrations on mm-wave channel: Doppler spread and correlative channel sounding," in *IEEE 27th Annual Int. Symp. on Personal, Indoor, and Mobile Radio Commu. (PIMRC)*, Sep. 2016, pp. 432–437.

[11] G. J. Foschini and M. J. Gans, "On limits of wireless communications in a fading environment when using multiple antennas," *Wireless personal communications*, vol. 6, no. 3, pp. 311–335, 1998.

[12] M. Rupp, J. A. Garcia-Naya, C. Mehlfuhrer, S. Caban, and L. Castedo, "On mutual information and capacity in frequency selective wireless channels," in *2010 IEEE International Conference on Communications (ICC)*, May 2010, pp. 1–5.